

Limits to Thermal Transport in Nanoscale Metal Bilayers due to Weak Electron-Phonon Coupling in Au and Cu

Wei Wang (汪维)* and David G. Cahill

Department of Materials Science and Engineering and Materials Research Laboratory, University of Illinois, Urbana, Illinois 61801, USA

(Received 16 June 2012; published 26 October 2012)

Weak electron-phonon coupling in Au and Cu produces a significant thermal resistance when heat flows from a thin Pt layer into a thin Au or Cu layer on picosecond time scales. Metal bilayers (Pt/Au and Pt/Cu) were prepared by magnetron sputter deposition; thermal transport in the bilayers was studied by time domain thermoreflectance in the temperature range $38 < T < 300$ K. Analysis of heat transfer in the bilayer yields the electron-phonon coupling parameter $g(T)$ of Au and Cu. Our results for $g(T)$ are consistent with the temperature dependence predicted by the two-temperature model of Kaganov *et al.* [Sov. Phys. JETP **4**, 173 (1957)] and help bridge the gap between data obtained using pump-probe spectroscopy at room temperature and electrical measurements at low temperatures.

DOI: [10.1103/PhysRevLett.109.175503](https://doi.org/10.1103/PhysRevLett.109.175503)

PACS numbers: 63.20.kd, 73.50.-h

Coupling between electronic and vibrational excitations underlies a wide variety of phenomena in materials physics: electrical resistance [1], superconductivity [2], hot-carrier mobility, phonon-drag thermopower [3], radiation damage [4], and the equilibration rate of an abruptly heated material [5]. The emerging field of spin caloritronics is creating a renewed interest in coupling between energy, spin, and charge degrees of freedom in materials [6–8]. The exchange of thermal energy between electronic and vibrational excitations is typically described by “two-temperature models” [2,9] that are based on an assumption that the occupation of electronic and vibrational excitations can be separately described by two effective temperatures, the electron temperature T_e and the lattice temperature T_l , and that the heat flux between electrons and phonons can be described by the product of a coupling parameter $g(T)$ and the temperature difference $(T_e - T_l)$.

Conventional approaches for measuring $g(T)$ in metals are ultrafast pump-probe optical spectroscopy at high temperatures, typically $T > 300$ K [10–15], and electrical measurements at low temperatures, typically $T < 4$ K [16–18]. In the ultrafast optics approach, a pump optical pulse creates a nonequilibrium distribution of electronic excitations. A time-delayed probe optical pulse measures the evolution of the electron temperatures through changes in optical absorption [19], optical reflectivity, or the strength of optical nonlinearities [20]. $g(T)$ is then derived from an analysis of the time-dependent signals and an estimate of the electronic heat capacity. In the electrical measurement approach, the temperature difference between the charge carriers and the lattice is derived from variations in the resistivity or current noise of a metal film as a function of electric field [16].

Electrical measurements of $g(T)$ cannot be easily extended to $T > 4$ K because the electrical power required to create a significant steady-state temperature difference

$(T_e - T_l)$ becomes large, and the change in the lattice temperature is not known accurately enough to determine $(T_e - T_l)$. On the other hand, ultrafast pump-probe measurements cannot be easily extended to $T < 300$ K because the equilibration time of the electronic system is not always well separated from the time scale for thermal equilibration between electrons and phonons [21,22]. This difficulty is aggravated at low temperatures because $k_B T$ becomes a smaller fraction of the photon energy. Groeneveld and co-workers measured the electron relaxation times in Au and Ag in the temperature range $10 < T < 300$ K [21]. Because of slow equilibration within the electronic system at low temperatures, they found relaxation times longer by a factor of 2–4 than the relaxation times predicted by a two-temperature model.

In our experiments, we also use ultrafast pump-probe measurements but approach the problem differently by indirectly heating the electrons in Au or Cu through contact with an abruptly heated layer of Pt. Pt has strong electron-phonon coupling—the electron-phonon coupling parameter of Pt is 40 times larger than Au at 300 K [5]—and, therefore, electrons and phonons in Pt equilibrate rapidly. The electronic thermal conductance of the Pt/Au interface is large and electrons in Au are nearly in equilibrium with the temperature of the Pt layer. Therefore, for short times after the Pt layer is heated, only the phonons in Au are out of equilibrium with the other excitations of the bilayer. We monitor the transfer of heat from the Pt layer through the Au electrons and into the Au lattice. In conventional pump-probe experiments, the relaxation time of the electron gas is given by the *electronic* heat capacity divided by $g(T)$; in our experiments, the equilibration time of the metal bilayer is on the order of the *lattice* heat capacity divided by $g(T)$, a nearly 2 orders of magnitude longer time scale. Our data for $g(T)$ closely follow the temperature dependence predicted by the 1957 two-temperature model of Kaganov

et al. [9]. The room-temperature values are $7.5 \times 10^{16} \text{ W m}^{-3} \text{ K}^{-1}$ for Cu and $2.8 \times 10^{16} \text{ W m}^{-3} \text{ K}^{-1}$ for Au. Elsayed-Ali and co-workers [12] previously reported $\sim 1 \times 10^{17} \text{ W m}^{-3} \text{ K}^{-1}$ for Cu. Electron-phonon coupling in Au near room temperature has been studied by many groups; reported values fall in the range $2 < g < 4 \times 10^{16} \text{ W m}^{-3} \text{ K}^{-1}$ [5,21,23,24].

We deposited metal bilayers on sapphire substrates by magnetron sputtering. We choose Pt as the base layer with strong electron-phonon coupling because the surface of Pt is relatively inert; i.e., the binding energy and reactive sticking coefficient of water vapor, the dominant residual gas in our deposition chamber, is small [25,26]. We also expect that H_2O , O_2 , and OH species that chemically react with the surface will mostly desorb during the deposition of the top layer since the metal-metal bonding is much stronger than the binding of these species to the metals. After the deposition of the Pt layer, we close a shutter in front of the sample, sputter the Au or Cu target for 20 s, and then open the shutter to deposit the top metal layer.

We have not attempted to characterize carbon or oxygen contamination of the buried interfaces—in general, characterization of light element contamination of interfaces is a challenging task. We do not require, however, that the interfaces are completely free of contaminants. We only require that the electronic thermal conductance of the interface [27,28] is sufficiently large; see the discussion below.

The base pressure of the chamber was $< 1 \times 10^{-7}$ Torr and the deposition rates of the metals were 10 nm/min. A 20 nm Pt layer deposited on sapphire had an electrical resistivity of $19 \pm 0.5 \mu\Omega \text{ cm}$, approximately twice the intrinsic value. Assuming that the electrical conduction in the bilayer acts in parallel, the electrical resistivities of the Au and Cu layers are 4.0 ± 0.5 and $4.3 \pm 0.5 \mu\Omega \text{ cm}$, respectively, and a factor of ≈ 2 larger than the intrinsic resistivity of the pure metals.

We used x-ray reflectivity (XRR) to determine thickness and the morphology. The Cu x-ray source has a beam divergence of 0.15 mrad. XRR data for the Pt/Au and Pt/Cu bilayers and model fits are shown in Fig. 1. The free parameters in the fits are the thickness of the metal layers, the roughness of the metal-metal interface σ_i , and the roughness of the top surface σ_s . For the Pt/Au bilayer, fits to the data give $\sigma_s = 0.47 \text{ nm}$, $h_{\text{Au}} = 20.6 \text{ nm}$, $\sigma_i = 0$, and $h_{\text{Pt}} = 20.2 \text{ nm}$. For the Pt/Cu bilayer, we find $\sigma_s = 1.3 \text{ nm}$, $h_{\text{Cu}} = 19.6 \text{ nm}$, $\sigma_i = 0.4 \text{ nm}$, and $h_{\text{Pt}} = 20.0 \text{ nm}$. The uncertainty of the thickness of metal layers is $< 1 \text{ nm}$. The small values of the surface and interface roughness confirm that the layer thicknesses are uniform and that the morphology of the Pt/Au and Pt/Cu interfaces are nearly planar.

We use time domain thermoreflectance (TDTR) to characterize heat transfer in the bilayer samples [29]. In a TDTR experiment, a pump optical pulse heats the sample

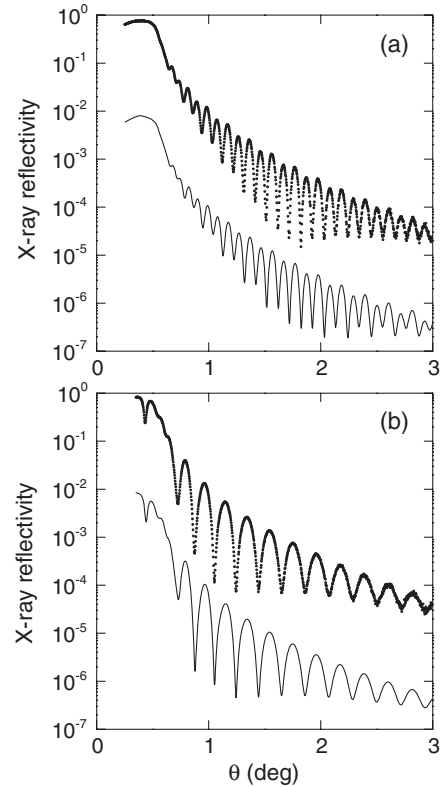


FIG. 1. X-ray reflectivity data (filled circles) and model fits (solid lines) for (a) Pt/Au sapphire and (b) Pt/Cu sapphire. The model fits are shifted down by a factor of 100 for clarity.

and the evolution of temperature in the sample is measured by a time-delayed probe pulse through the temperature dependence of the optical reflectivity. We pump and probe the bilayer from the Pt side; i.e., the pump and probe beams pass through the sapphire substrate. The rms radii of the focused beams are both $10.3 \mu\text{m}$. We calculate using a multilayer optical model that only a small fraction of the energy in the pump beam, $\approx 1\%$, is absorbed in the Au or Cu layer; the Pt layer absorbs $\approx 45\%$ of the energy. Measurements were carried out in an optical cryostat. A pump beam of 20 mW was used above 100 K; below 100 K, we used a pump laser power that is approximately proportional to temperature: 2 mW at 36 K increasing to 5 mW at 73 K. The power of the probe beam was 1/2 the power of the pump beam. The maximum temperature excursion (per pulse heating) of the Pt layer was always smaller than 13% and half of the maximum temperature excursion was added to the base temperature as a correction.

Because the metal layers are thin, even a small amount of ice condensed on the surface of the sample will make a significant contribution to the heat capacity. Therefore, we took precautions to avoid condensation. To eliminate line-of-sight deposition on the sample by outgassing from the walls of the cryostat, we drilled a small hole in the cold finger of the cryostat and placed the metal bilayer side of

the sample over this hole. We covered the other side of the hole by a glass slide to protect the sample surface. A small channel cut into the Cu cold finger allows gas to escape the space between the sample and the glass slide.

$g(T)$ is the thermal conductance per unit volume that describes the exchange of thermal energy between the electrons and phonons. In our experimental geometry, however, we also have to consider interfacial transport processes that act in parallel and series with this volumetric thermal conductance. To facilitate discussion and modeling of the data, we describe the equilibration of electrons and phonons in the top metal layer by an effective thermal conductance per unit area given by the product of $g(T)$ and the layer thickness h . The TDTR measurements are sensitive to $g(T)$ of the Au or Cu layer because $hg(T)$ is much smaller than the electronic thermal conductance of the interface G_{ee} , and much larger than the phonon-mediated thermal conductance of the interface G_{ph} . The conductance $hg(T)$ acts in series with G_{ee} and in parallel with G_{ph} . The characteristic length scale for electron-phonon equilibration at room temperature is $\sqrt{\Lambda_{el}/g} \approx 100$ nm in Au and ≈ 60 nm in Cu. Thus, the electron temperature in Au or Cu is approximately homogeneous in the 20 nm layer.

In most of our prior work using TDTR, we analyze the ratio of the in-phase and out-of-phase signals of the rf lock-in amplifier. However, because the out-of-phase signal becomes small at low temperatures, we found that a better approach in the present case is to analyze the in-phase signal normalized by the signal at 200 ps for the Pt/Au bilayer or at 125 ps for the Pt/Cu bilayer. These delay times are chosen by the times at which the metal bilayer has nearly equilibrated; see Fig. 2. The relatively low thermal conductance G_S of the Pt/sapphire interface inhibits heat flow into the substrate at short times, <300 ps. We use values for sapphire thermal conductivity from

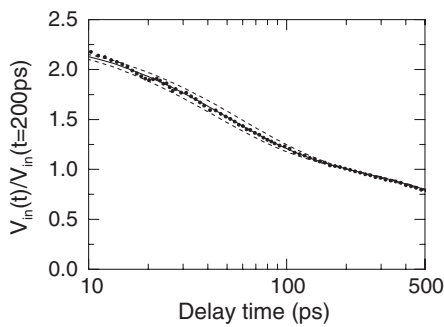


FIG. 2. In-phase thermoreflectance signal $V_{in}(t)$ for the Pt/Au sapphire sample plotted as a function of delay time between the pump and probe laser pulses. The data are normalized by the signal measured at a pump-probe delay time of $t = 200$ ps. The solid line is the best fit to the experimental data using $G_{tot} = 600$ MW m $^{-2}$ K $^{-1}$ as the total thermal conductance of the Pt/Au interface. The dashed lines are calculations using $G_{tot} = 500$ MW m $^{-2}$ K $^{-1}$ and $G_{tot} = 700$ MW m $^{-2}$ K $^{-1}$ to demonstrate the sensitivity of the measurement.

Ref. [30]. G_S is determined from the data at delay times >300 ps. Typical values of G_S of Pt/Au sapphire for temperatures of 40, 80, 160, and 300 K are 14, 39, 74, and 105 MW m $^{-2}$ K $^{-1}$, respectively. A 20% error in G_S propagates to less than a 7% error in g .

To analyze the TDTR data [29,31], we adjust two free parameters, the total thermal conductance G_{tot} that connects the Pt and Au layers and the thermal conductance of the Pt/sapphire interface. All other parameters, including the heat capacities and thicknesses of the Pt, Au, and Cu layers, and the heat capacity and thermal conductivity of the sapphire substrate, are fixed by literature values or separate measurements. G_{tot} is the series sum of G_{ee} and $hg(T)$ with a contribution from phonon conductance G_{ph} added in parallel:

$$G_{tot} = \frac{G_{ee}hg(T)}{G_{ee} + hg(T)} + G_{ph}. \quad (1)$$

Expanding Eq. (1) in the small parameters $hg(T)/G_{ee}$ and $G_{ph}/hg(T)$ gives

$$g(T) = \frac{G_{tot}}{h} \left(1 + \frac{hg(T)}{G_{ee}} - \frac{G_{ph}}{hg(T)} \right). \quad (2)$$

Thus, $g(T) \approx G_{tot}/h$ with small corrections due to the electronic and phononic thermal conduction of the interface that oppose each other.

We estimate G_{ee} using prior measurements of the specific electrical resistance AR of Pd/Cu ($AR = 0.36$ f Ω m 2) and Pd/Au ($AR = 0.23$ f Ω m 2) interfaces [32], the Wiedemann-Franz law for interfaces [28,33] $G_{ee} = L_0T/(AR)$, where L_0 is the Lorenz number, and the assumption that the specific resistance of the interface is independent of temperature [34]. Following this approach, $G_{ee} > 20$ GW m $^{-2}$ K $^{-1}$ at room temperature and the condition $G_{ee} \gg G_{tot}$ is well satisfied.

G_{ph} is more difficult to estimate from experiment because most experimental research on the phonon-mediated thermal conductance of interfaces has used interfaces between metals with dielectrics substrates with relatively high Debye temperatures [35–37]. An exception is BaF $_2$ studied by Stoner and Maris [35] who found $G_{ph} \approx 0.1$ GW m $^{-2}$ K $^{-1}$ near room temperature for Al/BaF $_2$ and Pb/BaF $_2$ and a smaller value, $G_{ph} \approx 0.04$ GW m $^{-2}$ K $^{-1}$, for Au/BaF $_2$, presumably due to weak interfacial bonding between Au and BaF $_2$ [38]. We conclude that $G_{ph} \ll G_{tot}$ and that the largest relative contribution of G_{ph} to G_{tot} is for the Pt/Au sample.

Our measurements of $g(T)$, see Fig. 3, agree well with the prediction of the two-temperature model developed in 1957 by Kaganov, Lifshitz, and Tanatarov [9]. The Kaganov theory is approximate: more rigorous treatments of electron-phonon coupling in metals are available [1,2], but the simple Kaganov theory appears to fit the data well and is straightforward to evaluate. The temperature dependence of the electron-phonon coupling parameter $g(T)$ is given by the functional form $F(T)$:

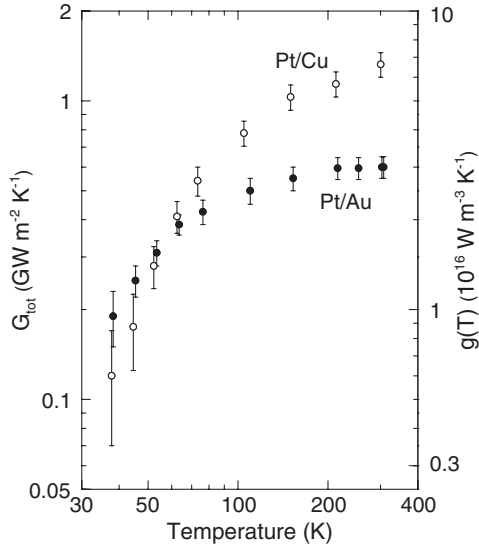


FIG. 3. Left axis: Thermal conductance G_{tot} of the Pt/Au (filled circles) and Pt/Cu (open circles) interfaces plotted as a function of temperature. Right axis: The electron-phonon coupling parameter $g(T) = G_{\text{tot}}/h$, with $h = 20$ nm.

$$F(T) = g_0 \frac{20T^4}{\Theta^4} \int_0^{\Theta/T} \frac{x^4 dx}{\exp(x) - 1} - \frac{4\Theta}{T[\exp(\Theta/T) - 1]}, \quad (3)$$

where Θ is the Debye temperature of Au (162 K) or Cu (347 K), and g_0 is the high temperature limit of g . The best fits to the $g(T)$ data give $g(300 \text{ K}) = 2.8 \times 10^{16} \text{ W m}^{-3} \text{ K}^{-1}$ for Au and $g(300 \text{ K}) = 7.5 \times 10^{16} \text{ W m}^{-3} \text{ K}^{-1}$ for Cu.

In the high temperature limit ($T \gg \Theta$) [2]:

$$g_0 = \frac{\pi^2}{6} \frac{m_e s^2 n_e}{\tau(T)T}, \quad (4)$$

where m_e is the effective mass, s the speed of sound, n_e the electron density, and $\tau(T)$ the relaxation time [5]. At high temperatures, $\tau(T)T$ is approximately constant; $m_e/[\tau(T)T]$ can be obtained from the electrical resistivity. Using the Debye speed of sound, $v_D = 2.65 \times 10^3 \text{ m s}^{-1}$ for Cu and $v_D = 1.40 \times 10^3 \text{ m s}^{-1}$ for Au, and assuming one free electron per atom, Eq. (4) predicts $g_0 = 2.1 \times 10^{16} \text{ W m}^{-3} \text{ K}^{-1}$ for Au and $g_0 = 1.2 \times 10^{17} \text{ W m}^{-3} \text{ K}^{-1}$ for Cu.

The fit of our data to Eq. (3) also allows us to make a connection to the values of $g(T)$ measured in low temperature experiments. In Fig. 4 we compare an extrapolation of the T^4 dependence of $g(T)$ measured below 1 K [16,39]. The extrapolated $g(T)$ are consistent with Eq. (3) to within 20%.

In summary, we have measured the electron-phonon coupling parameter $g(T)$ of Cu and Au over a wide temperature range, $38 < T < 300$ K, that is not accessible to either conventional pump-probe optical spectroscopy or

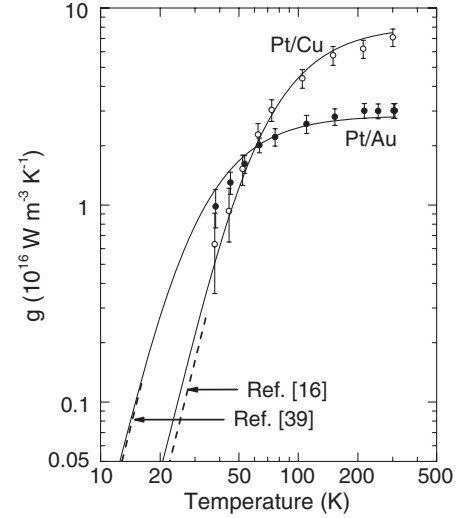


FIG. 4. Electron-phonon coupling parameter $g(T)$ of Au and Cu plotted as a function of lattice temperature with comparison to the Kaganov theory [9] [Eq. (3) solid lines]. Extrapolations of low temperature measurements (dashed lines) for Cu [16] and Au [39] extend to 1/10 of the Debye temperatures. These extrapolations assume a T^4 scaling in the low T limit.

electrical noise measurements. The temperature dependence of the data is consistent with the approximate theory of Kaganov *et al.* and a T^4 extrapolation of data for $g(T)$ previously measured in low temperature experiments.

We thank Dana Dlott and Brandt Pein for their insights on indirect heating of thin Au layers, Kaiping Tai for assistance with sputter deposition, and Richard Wilson for helpful discussions. This work was supported by the U.S. Department of Energy Office of Basic Energy Sciences, under Grant No. DE-FG02-07ER46459, and was carried out in the Laser and Spectroscopy Laboratory of the Materials Research Laboratory at the University of Illinois Urbana-Champaign.

*wang302@illinois.edu

- [1] J. Ziman, *Proc. R. Soc. A* **226**, 436 (1954).
- [2] P. B. Allen, *Phys. Rev. Lett.* **59**, 1460 (1987).
- [3] C. Herring, *Phys. Rev.* **96**, 1163 (1954).
- [4] C. Race, D. Mason, M. Finnis, W. Foulkes, A. Horsfield, and A. Sutton, *Rep. Prog. Phys.* **73**, 116501 (2010).
- [5] Z. Lin, L. V. Zhigilei, and V. Celli, *Phys. Rev. B* **77**, 075133 (2008).
- [6] G. E. W. Bauer, E. Saitoh, and B. J. van Wees, *Nature Mater.* **11**, 391 (2012).
- [7] J. Sinova, *Nature Mater.* **9**, 880 (2010).
- [8] J. Xiao, G. E. W. Bauer, K. C. Uchida, E. Saitoh, and S. Maekawa, *Phys. Rev. B* **81**, 214418 (2010).
- [9] M. I. Kaganov, I. M. Lifshitz, and L. V. Tanatarov, *Sov. Phys. JETP* **4**, 173 (1957).
- [10] S. D. Brorson, J. G. Fujimoto, and E. P. Ippen, *Phys. Rev. Lett.* **59**, 1962 (1987).

- [11] C.K. Sun, F. Vallee, L.H. Acioli, E.P. Ippen, and J.G. Fujimoto, *Phys. Rev. B* **50**, 15 337 (1994).
- [12] H.E. Elsayed-Ali, T.B. Norris, M.A. Pessot, and G.A. Mourou, *Phys. Rev. Lett.* **58**, 1212 (1987).
- [13] W.S. Fann, R. Storz, H.W.K. Tom, and J. Bokor, *Phys. Rev. B* **46**, 13 592 (1992).
- [14] P.E. Hopkins, L.M. Phinney, and J.R. Serrano, *J. Heat Transfer* **133**, 044505 (2011).
- [15] C. Gadermaier, A. S. Alexandrov, V. V. Kabanov, P. Kusar, T. Mertelj, X. Yao, C. Manzoni, D. Brida, G. Cerullo, and D. Mihailovic, *Phys. Rev. Lett.* **105**, 257001 (2010).
- [16] M.L. Roukes, M.R. Freeman, R.S. Germain, R.C. Richardson, and M.B. Ketchen, *Phys. Rev. Lett.* **55**, 422 (1985).
- [17] M. Nahum and J.M. Martinis, *Appl. Phys. Lett.* **63**, 3075 (1993).
- [18] F.C. Wellstood, C. Urbina, and J. Clarke, *Phys. Rev. B* **49**, 5942 (1994).
- [19] R.H.M. Groeneveld, R. Sprik, and A. Lagendijk, *Phys. Rev. Lett.* **64**, 784 (1990).
- [20] J. Hohlfeld, D. Grosenick, U. Conrad, and E. Matthias, *Appl. Phys. A* **60**, 137 (1995).
- [21] R.H.M. Groeneveld, R. Sprik, and A. Lagendijk, *Phys. Rev. B* **51**, 11 433 (1995).
- [22] G. Tas and H.J. Maris, *Phys. Rev. B* **49**, 15 046 (1994).
- [23] J. Hohlfeld, S.S. Wellershoff, J. Güdde, U. Conrad, V. Jähnke, and E. Matthias, *Chem. Phys.* **251**, 237 (2000).
- [24] J.H. Hodak, A. Henglein, and G.V. Hartland, *J. Chem. Phys.* **112**, 5942 (2000).
- [25] J.L. Daschbach, B.M. Peden, R.S. Smith, and B.D. Kay, *J. Chem. Phys.* **120**, 1516 (2004).
- [26] H. Wang, J. Biesecker, M. Iedema, G. Ellison, and J. Cowin, *Surf. Sci.* **381**, 142 (1997).
- [27] B.C. Gundrum, D.G. Cahill, and R.S. Averback, *Phys. Rev. B* **72**, 245426 (2005).
- [28] R.B. Wilson and D.G. Cahill, *Phys. Rev. Lett.* **108**, 255901 (2012).
- [29] D.G. Cahill, *Rev. Sci. Instrum.* **75**, 5119 (2004).
- [30] Y.S. Touloukian, R.W. Powell, C.Y. Ho, and P.G. Klemens, *Thermal Conductivity Nonmetallic Solids*, Thermophysical Properties of Matter Vol. 2 (Plenum, New York, 1970), p. 97.
- [31] A.J. Schmidt, X. Chen, and G. Chen, *Rev. Sci. Instrum.* **79**, 114902 (2008).
- [32] C. Galinon, *Appl. Phys. Lett.* **86**, 182502 (2005).
- [33] G. Mahan and M. Bartkowiak, *Appl. Phys. Lett.* **74**, 953 (1999).
- [34] W. Pratt and J. Bass, *Appl. Surf. Sci.* **256**, 399 (2009).
- [35] R.J. Stoner and H.J. Maris, *Phys. Rev. B* **48**, 16 373 (1993).
- [36] R.J. Stevens, A.N. Smith, and P.M. Norris, *J. Heat Transfer* **127**, 315 (2005).
- [37] H.K. Lyeo and D.G. Cahill, *Phys. Rev. B* **73**, 144301 (2006).
- [38] W.P. Hsieh, B. Chen, J. Li, P. Keblinski, and D.G. Cahill, *Phys. Rev. B* **80**, 180302 (2009).
- [39] A. Mocharnuk-Macchia, Y. Kim, H. Eguchi, Y. Huang, R. Lanou, H. Maris, G. Seidel, B. Sethumadhavan, and W. Yao, *AIP Conf. Proc.* **850**, 1603 (2006).